

# FAST SOLUTION OF INCOMPRESSIBLE FLOW PROBLEMS WITH TWO-LEVEL PRESSURE APPROXIMATION

JENNIFER PESTANA AND DAVID J. SILVESTER

**ABSTRACT.** This paper develops efficient preconditioned iterative solvers for incompressible flow problems discretised by an enriched Taylor–Hood mixed approximation, in which the usual pressure space is augmented by a piecewise constant pressure to ensure local mass conservation. This enrichment process causes over-specification of the pressure, which complicates the design and implementation of efficient solvers for the resulting linear systems. We first describe the impact of this choice of pressure space on the matrices involved. Next, we show how to recover effective solvers for Stokes problems, with a preconditioner based on the singular pressure mass matrix, and for Oseen systems arising from linearised Navier–Stokes equations, by using a two-stage pressure convection–diffusion strategy. The codes used to generate the numerical results are available online.

## 1. INTRODUCTION

Reliable and efficient iterative solvers for models of steady incompressible flow emerged in the early 1990s. Strategies based on block preconditioning of the underlying matrix operators using (algebraic or geometric) multigrid components have proved to be the key to realising mesh independent convergence (and optimal complexity) without the need for tuning parameters, particularly in the context of classical mixed finite element approximation, see Elman et al. [5, chap. 9]. The focus of this contribution is on efficient solver strategies in cases where (an inf–sup) stable Taylor–Hood mixed approximation is augmented by a piecewise constant pressure in order to guarantee local conservation of mass. The augmentation leads to over-specification of the pressure solution requiring a redesign of the established solver technology.

The idea of adding a piecewise constant pressure to the standard rectangular biquadratic velocity, bilinear pressure ( $\mathbb{Q}_2\text{--}\mathbb{Q}_1$ ) approximation was originally suggested during discussion around a blackboard at a conference on finite elements in fluids held in Banff in 1980; see Gresho et al. [6]. The need for local mass conservation was motivated by competition from finite volume methods (such as the MAC scheme) in the design of effective strategies for modelling buoyancy-driven flow in the atmosphere.

The extension of the augmentation idea to Taylor–Hood ( $\mathbb{P}_2\text{--}\mathbb{P}_1$ ) triangular approximation was proposed in a paper presented at a conference in Reading in 1982; see Griffiths [7]. A proof of stability of the augmented  $\mathbb{P}_2\text{--}\mathbb{P}_1$  approximation on triangular meshes was constructed by Thatcher & Silvester [16] in 1987. An extended version of this manuscript included discussion of  $\mathbb{Q}_2\text{--}\mathbb{Q}_1$  hexahedral elements [15]. A rigorous assessment of the augmentation strategy was undertaken by Boffi et al. two decades later [4]. The strategy of augmenting a continuous pressure approximation to give a locally mass-conserving

---

*Date:* March 21, 2023.

*Acknowledgements.* This work was supported by EPSRC grant EP/W033801/1.

strategy can also be generalised to higher-order  $\mathbb{Q}_k\text{--}\mathbb{Q}_{k-1}$  and  $\mathbb{P}_k\text{--}\mathbb{P}_{k-1}$  Taylor–Hood approximations. Inf–sup stability is assured for  $k \geq 2$  in two dimensions and for  $\mathbb{P}_k\text{--}\mathbb{P}_{k-1}$  with  $k \geq 3$  in three dimensions; see [3, p. 506].

The novel contribution in this work lies in the linear algebra aspects of two-field pressure approximation. The immediate issue that needs to be dealt with is the fact that the mass matrix that determines the *stability* of the resulting mixed approximation is *singular*. This aspect is discussed in section 2. The main issue that has to be dealt with in practical flow simulation is the over-specification and associated ill-conditioning of the discrete operators that arise in the preconditioning of the linearised Navier–Stokes operator. This is the focus of the discussion in section 3. The conclusion of this study is that *optimal* complexity convergence rates can be recovered when using two-field pressure approximation, but only after a careful redesign of the preconditioning components.

## 2. TWO-FIELD PRESSURE MASS MATRIX

In this section we consider the Stokes problem

$$\begin{aligned} -\Delta \vec{u} + \nabla p &= \vec{f} & \text{in } \Omega, \\ \nabla \cdot \vec{u} &= 0 & \text{in } \Omega, \\ \vec{u} &= \vec{g} & \text{on } \partial\Omega, \end{aligned}$$

where  $\vec{u}$  and  $p$  are the fluid velocity and pressure, respectively, and  $\Omega \subset \mathbb{R}^d$ ,  $d \in \{2, 3\}$ , is a polygonal or polyhedral domain.

Throughout this section, we assume that  $\mathbf{V}_h \subset H_0^1(\Omega)^d$  and  $Q_h \subset L_0^2(\Omega) := \{q \in L_2 : \int_{\Omega} q = 0\}$  are an inf–sup stable pair of finite element spaces. Then the corresponding finite element approximation problem is to find  $(\vec{u}_h, p_h) \in \mathbf{V}_h \times Q_h$  such that

$$a(\vec{u}_h, \vec{v}_h) + b(\vec{v}_h, p_h) = (\vec{f}, \vec{v}_h) \quad \text{for all } \vec{v}_h \in \mathbf{V}_h, \quad (1a)$$

$$b(\vec{u}_h, q_h) = 0 \quad \text{for all } q_h \in Q_h, \quad (1b)$$

where  $(\cdot, \cdot)$  denotes the usual  $L^2$  inner product, and

$$a(\vec{u}, \vec{v}) = \int_{\Omega} \nabla \vec{u} : \nabla \vec{v}, \quad b(\vec{u}, p) = - \int_{\Omega} p \nabla \cdot \vec{u}.$$

Solving the finite element problem (1) is then equivalent to solving the linear system

$$\underbrace{\begin{bmatrix} \mathbf{A} & B^T \\ B & 0 \end{bmatrix}}_{\mathcal{A}} \begin{bmatrix} \mathbf{u} \\ p \end{bmatrix} = \begin{bmatrix} \mathbf{f} \\ \mathbf{g} \end{bmatrix}, \quad (2)$$

where  $\mathbf{A} \in \mathbb{R}^{n_u \times n_u}$  is symmetric positive definite and  $B \in \mathbb{R}^{n_p \times n_u}$  [5, chap. 3]. The matrix  $\mathcal{A}$  is of well-known saddle point type, and solvers for this sort of system have been extensively studied, see, e.g., Benzi et al. [1]. Since  $\mathcal{A}$  is large and sparse, the system is typically solved by an iterative method, with preconditioned MINRES [12] a popular choice.

An ideal preconditioner for  $\mathcal{A}$  is [10, 11]

$$\mathcal{P}_{\text{ideal}} = \begin{bmatrix} \mathbf{A} & \\ & B\mathbf{A}^{-1}B^T \end{bmatrix},$$

since the eigenvalues of the preconditioned matrix are 0, 1, and  $(1 \pm \sqrt{5})/2$ , with the zero eigenvalue appearing only if the preconditioned matrix is singular. This preconditioner is usually too costly to apply, and so efficient block diagonal preconditioners for  $\mathbf{A}$  are typically based on spectrally equivalent preconditioners for  $\mathbf{A}$  and the negative Schur complement  $S = B\mathbf{A}^{-1}B^T$ . For Stokes problems, the solve with  $\mathbf{A}$  can be replaced by, e.g., an algebraic or geometric multigrid solver, while for stable discretisations  $S$  is spectrally equivalent to  $Q^*$ , the pressure mass matrix [5, chap. 3], i.e., there exist constants  $\gamma$  and  $\Gamma$ , independent of  $h$ , such that

$$\gamma^2 \leq \frac{\mathbf{q}^T B\mathbf{A}^{-1}B^T \mathbf{q}}{\mathbf{q}^T Q^* \mathbf{q}} \leq \Gamma^2 \quad (3)$$

for all vectors  $\mathbf{q}$  except those corresponding to the function  $q_h \equiv 1$  on  $\Omega$ . For certain element pairs,  $Q^*$  itself is easily inverted, e.g., for discontinuous  $\mathbb{P}_0$  or  $\mathbb{Q}_0$  pressures, the mass matrix is diagonal. Otherwise,  $Q^*$  can be replaced by its diagonal or by a fixed number of steps of Chebyshev semi-iteration when, as is common,  $\text{diag}(Q^*)^{-1}Q^*$  has eigenvalues within a small interval and this interval lies away from the origin [17, 18].

To summarise, for inf-sup stable finite element pairs, an effective preconditioner for (2) is

$$\mathcal{P} = \begin{bmatrix} \mathbf{M} & \\ & M_S \end{bmatrix}, \quad (4)$$

where  $\mathbf{M} \in \mathbb{R}^{n_u \times n_u}$  is  $\mathbf{A}$  or an approximation, and  $M_S \in \mathbb{R}^{n_p \times n_p}$  is  $Q^*$  or an approximation. (See, e.g., Elman et al. [5, chap. 4] for results with  $\mathbb{Q}_2$ - $\mathbb{Q}_1$  approximation on quadrilaterals).

In this section, our aim is to determine effective preconditioners for the enriched Taylor–Hood element. As we will see, although enriching the pressure space results in better mass conservation properties, it also presents challenges for solving (2).

**2.1. Augmented Taylor–Hood Elements.** We see from (1) that the mass conservation condition  $\nabla \cdot \vec{u} = 0$  is imposed only in a weak sense, and if Taylor–Hood elements are employed we can only guarantee that (1b) will hold. However, by augmenting the pressure space by piecewise constant pressures it is possible to obtain local mass conservation, so that the average of the divergence is zero on each individual element. However, as we will discuss later in this section, a consequence is that constant pressures have multiple representations, and this results in certain challenges for solving (2).

Let us now describe the enriched Taylor–Hood finite element spaces. We first introduce a shape-regular family of simplicial, quadrilateral (in 2D) or hexahedral (in 3D) decompositions of the domain  $\Omega$ . We assume that any two elements have at most a common face, edge, or vertex and denote by  $h$  the maximum diameter of any element. The total number of elements in the resulting mesh is  $n_{el}$ .

We denote the usual Taylor–Hood finite element space by  $\mathbf{V}_h^{TH} \times Q_h^{TH}$ , so that  $\mathbf{V}_h^{TH} \times Q_h^{TH} = (\mathbb{Q}_{k+1})^d \times \mathbb{Q}_k$  or  $\mathbf{V}_h^{TH} \times Q_h^{TH} = (\mathbb{P}_{k+1})^d \times \mathbb{P}_k$  with  $d \geq 2$ . In the latter case, we additionally assume that the polynomial degree,  $k$ , satisfies  $k \geq d - 1$ . The corresponding enriched Taylor–Hood space is  $\mathbf{V}_h^{TH} \times Q_h^*$  where

$$Q_h^* = \{q = q_k + q_0, q_k \in Q_h^{TH}, q_0 \in Q_h^0\} \quad (5)$$

and  $Q_h^0$  is the space of discontinuous pressures that are constant on each element. Thus, we see that the velocity approximation space is identical to that of the corresponding

Taylor–Hood element, while  $Q_h^*$  is  $Q_h^{TH}$  augmented with piecewise constant pressures. It follows that functions in  $Q_h^*$  may be discontinuous across inter-element boundaries.

From a linear algebra perspective, a critical point is that any constant function on  $\Omega$  can be represented by a function in  $Q_h^{TH}$  or a function in  $Q_h^0$ . In other words, any constant function  $\beta$  on  $\Omega$  can be written as  $p = p_k + p_0 \in Q_h^*$ , where  $p_k \equiv \alpha \in Q_h^{TH}$  and  $p_0 \equiv \beta - \alpha \in Q_h^0$  on  $\Omega$ , for any  $\alpha \in \mathbb{R}$ . This has profound consequences for the linear algebra: the pressure mass matrix  $Q^*$  that determines  $M_S$  in (4) becomes singular, and the rank of the matrix  $B^T$  is reduced. These properties are established in the rest of this section.

We first let

$$Q_h^* = \text{span}\{\phi_1, \dots, \phi_{n_k}, \phi_{n_k+1}, \dots, \phi_{n_p}\}, \quad (6)$$

where  $\{\phi_k\}_{k=1}^{n_k}$  and  $\{\phi_k\}_{k=n_k+1}^{n_p}$  are Lagrange bases of  $Q_h^{TH}$  and  $Q_h^0$  (see (5)). This enables us to relate vectors  $\mathbf{p} \in \mathbb{R}^{n_p}$  and functions  $p = p_k + p_0 \in Q_h^*$ , where  $p_k \in Q_h^{TH}$ ,  $p_0 \in Q_h^0$ . Specifically,

$$p = \sum_{i=1}^{n_p} \mathbf{p}_i \phi_i, \quad p_k = \sum_{i=1}^{n_k} \mathbf{p}_i \phi_i \quad \text{and} \quad p_0 = \sum_{i=n_k+1}^{n_p} \mathbf{p}_i \phi_i. \quad (7)$$

As mentioned above, any constant function has multiple representations in  $Q_h^*$ . In particular, for any  $\alpha \in \mathbb{R}$ , setting  $p_k = \alpha$  and  $p_0 = -\alpha$  gives that  $p = p_k + p_0 \equiv 0$ . We see from (7) that this representation of the zero function corresponds to the vector  $\alpha \mathbf{k}$ , where

$$\mathbf{k} = \begin{bmatrix} \mathbf{1}_{n_k} \\ -\mathbf{1}_{n_0} \end{bmatrix} \quad (8)$$

and  $n_0 = n_p - n_k$ .

A direct consequence of the correspondence between  $\mathbf{k}$  and the zero function on  $\Omega$  is that  $Q^* \mathbf{k} = \mathbf{0}$  and  $B^T \mathbf{k} = \mathbf{0}$ , as we now show.

**Proposition 1.** *Let*

$$Q^* = [q_{ij}]_{i,j=1}^{n_p}, \quad q_{ij} = \int_{\Omega} \phi_i \phi_j,$$

*be the pressure mass matrix for the enriched Taylor–Hood pressure space  $Q_h^*$  in (5), with basis functions (6). Then,  $\text{null}(Q^*) = \text{span}\{\mathbf{k}\}$ , where  $\mathbf{k}$  is given in (8).*

*Proof.* Let  $\mathbf{p} \in \mathbb{R}^{n_p}$ ,  $\mathbf{p} \neq \mathbf{0}$ . Then, using (7), we find that

$$\begin{aligned} Q^* \mathbf{p} = 0 &\Leftrightarrow \mathbf{p}^T Q^* \mathbf{p} = 0 \\ &\Leftrightarrow \int_{\Omega} \left( \sum_{i=1}^{n_p} \mathbf{p}_i \phi_i \right) \left( \sum_{j=1}^{n_p} \mathbf{p}_j \phi_j \right) = 0 \\ &\Leftrightarrow \int_{\Omega} p^2 = 0 \quad \Leftrightarrow p \equiv 0 \text{ in } \Omega, \end{aligned}$$

since  $p$  is continuous on each element.

As we have already seen in this section,  $p \equiv 0$  corresponds to the vector  $\alpha \mathbf{k}$ . This shows that  $\text{span}\{\mathbf{k}\} \subseteq \text{null}(Q^*)$ . We now show that there are no other vectors in the nullspace. Since  $p = p_k + p_0$ ,  $p_k \in Q_h^{TH}$ ,  $p_0 \in Q_h^0$ , we see that  $p_k = -p_0$  everywhere in  $\Omega$ . Moreover,  $p_0$  is constant on each element  $T$ ,  $T = 1, \dots, n_{el}$ , so  $p_0 \equiv \alpha_T$  on  $T$  for some constant  $\alpha_T \in \mathbb{R}$ . Hence,  $p_k \equiv -\alpha_T$  on  $T$ . However,  $p_k$  is continuous on  $\bar{\Omega}$ , and so it is

straightforward to see that  $\alpha_1 = \alpha_2 = \dots = \alpha_{n_{el}}$ , i.e., that  $p_0 \equiv \alpha$  and  $p_k \equiv -\alpha$  on  $\Omega$  for some constant  $\alpha \in \mathbb{R}$ . Such functions correspond to vectors of the form  $\alpha \mathbf{k}$ , which shows that  $\text{null}(Q^*) = \text{span}\{\mathbf{k}\}$ , as required.  $\square$

A very similar argument shows that  $\mathbf{k} \in \text{null}(B^T)$ .

**Proposition 2.** *Let  $B \in \mathbb{R}^{n_p \times n_u}$  in (2) be obtained from the enriched Taylor–Hood space  $\mathbf{V}_h^{TH} \times Q_h^*$ , using the basis functions for  $Q_h^*$  in (6). Then,  $\mathbf{k} \in \text{null}(B^T)$ , where  $\mathbf{k}$  is given in (8).*

*Proof.* For any  $\mathbf{v} \in \mathbb{R}^{n_u}$ , we have that

$$\mathbf{v}^T B^T \mathbf{k} = \mathbf{k}^T B \mathbf{v} = \int_{\Omega} p \nabla \cdot \vec{v}$$

with  $\vec{v} \in \mathbf{V}_h^{TH}$ . Additionally, from (7) and (8) it is clear that

$$p = \sum_{i=1}^{n_k} \mathbf{k}_i \phi_i + \sum_{i=n_k+1}^{n_p} \mathbf{k}_i \phi_i = \sum_{i=1}^{n_k} \phi_i - \sum_{i=n_k+1}^{n_p} \phi_i$$

is identically zero, so that  $\mathbf{v}^T B^T \mathbf{k} = 0$ . Since  $\mathbf{v}$  was arbitrarily chosen, we conclude that  $B^T \mathbf{k} = \mathbf{0}$ .  $\square$

What do these results mean for the solution of (2) by preconditioned MINRES? First, if  $B^T \mathbf{k} = \mathbf{0}$  then it follows that  $\mathcal{A}$  is always singular, with  $\mathcal{A} \mathbf{w} = \mathbf{0}$ , where

$$\mathbf{w} = \begin{bmatrix} \mathbf{0}_{n_u} \\ \mathbf{k} \end{bmatrix}. \quad (9)$$

If the linear system (2) is consistent then this does not pose a problem for preconditioned MINRES. However, as we shall now see, the proposed block diagonal preconditioner (4), with  $M_G = Q^*$ , is also singular, and this is potentially problematic.

**Algorithm 3.** Preconditioned MINRES algorithm for solving  $\mathcal{A} \mathbf{x} = \mathbf{b}$  with symmetric positive definite preconditioner  $\mathcal{P}$  [5, Algorithm 4.1].

- 1:  $\mathbf{v}^{(0)} = \mathbf{0}$ ,  $\mathbf{w}^{(0)} = \mathbf{0}$ ,  $\mathbf{w}^{(1)} = \mathbf{0}$ ,  $\gamma_0 = 0$
- 2: Choose  $\mathbf{x}^{(0)}$ , compute  $\mathbf{v}^{(1)} = \mathbf{b} - \mathcal{A} \mathbf{x}^{(0)}$
- 3: Solve  $\mathcal{P} \mathbf{z}^{(1)} = \mathbf{v}^{(1)}$ , set  $\gamma_1 = \sqrt{\langle \mathbf{z}^{(1)}, \mathbf{v}^{(1)} \rangle}$
- 4: Set  $\eta = \gamma_1$ ,  $s_0 = s_1 = 0$ ,  $c_0 = c_1 = 1$
- 5: **for**  $j = 1$  until convergence **do**
- 6:      $\mathbf{z}^{(j)} = \mathbf{z}^{(j)} / \gamma_j$
- 7:      $\delta_j = \langle \mathcal{A} \mathbf{z}^{(j)}, \mathbf{z}^{(j)} \rangle$
- 8:      $\mathbf{v}^{(j+1)} = \mathcal{A} \mathbf{z}^{(j)} - (\delta_j / \gamma_j) \mathbf{v}^{(j)} - (\gamma_j / \gamma_{j-1}) \mathbf{v}^{(j-1)}$
- 9:     Solve  $\mathcal{P} \mathbf{z}^{(j+1)} = \mathbf{v}^{(j+1)}$
- 10:      $\gamma_{j+1} = \sqrt{\langle \mathbf{z}^{(j+1)}, \mathbf{v}^{(j+1)} \rangle}$
- 11:      $\alpha_0 = c_j \delta_j - c_{j-1} s_j \gamma_j$
- 12:      $\alpha_1 = \sqrt{\alpha_0^2 + \gamma_{j+1}^2}$
- 13:      $\alpha_2 = s_j \delta_j + c_{j-1} c_j \gamma_j$
- 14:      $\alpha_3 = s_{j-1} \gamma_j$
- 15:      $c_{j+1} = \alpha_0 / \alpha_1$ ;  $s_{j+1} = \gamma_{j+1} / \alpha_1$
- 16:      $\mathbf{w}^{(j+1)} = (\mathbf{z}^{(j)} - \alpha_3 \mathbf{w}^{(j-1)} - \alpha_2 \mathbf{w}^{(j)}) / \alpha_1$

```

17:    $\mathbf{x}^{(j)} = \mathbf{x}^{(j-1)} + c_{j+1}\eta\mathbf{w}^{(j+1)}$ 
18:    $\eta = -s_{j+1}\eta$ 
19:   <Test for convergence>
20: end for

```

**2.2. Dealing with a singular preconditioner.** Knowing that the enriched Taylor–Hood element is inf–sup stable implies that the preconditioner (4) will be effective when solving (2). However, the matrix  $Q^*$ , and hence the preconditioner  $\mathcal{P}$ , are singular, since  $\mathcal{P}\mathbf{w} = \mathbf{0}$ , where  $\mathbf{w}$  is given in (9). (Note that this implies that  $\mathcal{A}$  and  $\mathcal{P}$  have a common nullspace.)

To better understand the effect of a singular preconditioner  $\mathcal{P}$ , we need to explore the components of the preconditioned MINRES method that is presented in Algorithm 3. Specifically, we note that at each iteration step we need to solve a linear system of the form  $\mathcal{P}\mathbf{z}^{(j)} = \mathbf{v}^{(j)}$ . If this system is consistent there are infinitely many solutions, which take the form  $\mathbf{z}^{(j)} = \bar{\mathbf{z}}^{(j)} + \zeta_j\mathbf{w}$ , with  $\bar{\mathbf{z}}^{(j)} \perp \mathbf{w}$  and  $\zeta_j \in \mathbb{R}$ .

Let us examine the effect of  $|\zeta_j|$  on the scalars and vectors computed in Algorithm 3. First, note that if the linear system  $\mathcal{A}\mathbf{x} = \mathbf{b}$  is consistent then, since  $\mathcal{A}$  is symmetric,  $\mathbf{b} \perp \mathbf{w}$  and so  $\mathbf{v}^{(1)} \perp \mathbf{w}$ . It then follows by induction that  $\mathbf{v}^{(j)} \perp \mathbf{w}$ ,  $j = 1, 2, \dots$ , and that the systems  $\mathcal{P}\mathbf{z}^{(j)} = \mathbf{v}^{(j)}$  are all consistent. Furthermore,  $\gamma_j = \langle \mathbf{z}^{(j)}, \mathbf{v}^{(j)} \rangle^{\frac{1}{2}} = \langle \bar{\mathbf{z}}^{(j)}, \mathbf{v}^{(j)} \rangle^{\frac{1}{2}}$  because of the orthogonality of  $\mathbf{v}^{(j)}$  and  $\mathbf{w}$ , so that  $\zeta_j$  does not affect  $\gamma_j$ . Similarly,  $\delta_j = \langle \mathcal{A}\mathbf{z}^{(j)}, \mathbf{z}^{(j)} \rangle = \langle \mathcal{A}\bar{\mathbf{z}}^{(j)}, \bar{\mathbf{z}}^{(j)} \rangle$ , which shows that  $\delta_j$  is similarly unaffected by  $\zeta_j$ . Indeed, the only quantities that are affected by the nullspace components  $\zeta_j\mathbf{w}$ ,  $j = 1, 2, \dots$ , are the vectors  $\mathbf{w}^{(j)}$  and  $\mathbf{x}^{(j)}$ . In exact arithmetic, this is not a problem, since solutions of  $\mathcal{A}\mathbf{x} = \mathbf{b}$  may certainly contain a component in the direction of  $\mathbf{w}$ . However, in unlucky cases, the size of the nullspace component of  $\mathbf{x}^{(j)}$  may be so large as to dominate the approximate solution. Alternatively, in finite precision  $\mathbf{v}^{(j)}$  and  $\mathbf{w}$  may not be exactly orthogonal. Hence, it may be wise to explicitly ensure that  $\mathbf{z} \perp \mathbf{w}$ . One option is to orthogonalise  $\mathbf{z}$  against  $\mathbf{w}$  after each preconditioner solve, but if  $|\zeta_j|$  is large then the result may be inaccurate. A more robust approach is to note that solutions of  $\mathcal{P}\mathbf{z} = \mathbf{r}$  are minimisers of the quadratic form

$$\frac{1}{2}\mathbf{z}^T\mathcal{P}\mathbf{z} - \mathbf{z}^T\mathbf{r},$$

since  $\mathcal{P}$  is positive semidefinite. Constraining  $\mathbf{z}$  to be orthogonal to  $\mathbf{w}$  is then equivalent to the following optimisation problem:

$$\min_{\mathbf{z}} \frac{1}{2}\mathbf{z}^T\mathcal{P}\mathbf{z} - \mathbf{z}^T\mathbf{r} \quad \text{s.t.} \quad \mathbf{w}^T\mathbf{z} = 0.$$

Applying a Lagrange multiplier approach results in the augmented system

$$\begin{bmatrix} \mathcal{P} & \mathbf{w} \\ \mathbf{w}^T & 0 \end{bmatrix} \begin{bmatrix} \mathbf{z} \\ \lambda \end{bmatrix} = \begin{bmatrix} \mathbf{r} \\ 0 \end{bmatrix},$$

where  $\lambda$  is the Lagrange multiplier, and solving this augmented system gives a vector  $\mathbf{z}$  that is orthogonal to  $\mathbf{w}$ . Moreover, since

$$\begin{bmatrix} \mathcal{P} & \mathbf{w} \\ \mathbf{w}^T & 0 \end{bmatrix} = \begin{bmatrix} \mathbf{M} & 0 & 0 \\ 0 & M_S & \mathbf{k} \\ 0 & \mathbf{k}^T & 0 \end{bmatrix}$$

we see that only the solve with  $M_S$  needs to be modified.

**2.3. Approximating the two-level pressure mass matrix.** Now let us consider approximations of the matrix  $Q^*$  which, because of the two-level pressure approximation, has  $2 \times 2$  block structure:

$$Q^* = \begin{bmatrix} Q_k & R^T \\ R & Q_0 \end{bmatrix},$$

where

$$\begin{aligned} Q_k &= [q_{k,ij}], \quad i, j = 1, \dots, n_k, & q_{k,ij} &= \int_{\Omega} \phi_j \phi_i, \\ R &= [r_{ij}], \quad i = n_k + 1, \dots, n_p, \quad j = 1, \dots, n_k, & r_{ij} &= \int_{\Omega} \phi_j \phi_i, \\ Q_0 &= [q_{0,ij}], \quad i, j = n_k + 1, \dots, n_p, & q_{0,ij} &= \int_{\Omega} \phi_j \phi_i. \end{aligned}$$

Note that  $Q_k$  is the standard Taylor–Hood pressure mass matrix, and  $Q_0$  is the standard discontinuous pressure mass matrix, while  $R$  represents cross terms between the spaces  $Q_h^{TH}$  and  $Q_h^0$  (see (5)).

As discussed at the start of this section,  $Q_0$  is diagonal, and hence easy to invert, while good approximations of  $Q_k$  based on its diagonal or Chebyshev semi-iteration are known. However, the presence of the matrix  $R$  in  $Q^*$  complicates matters considerably. For example, replacing  $Q_k$  by its diagonal or Chebyshev semi-iteration results in mesh-dependent convergence rates and high iteration counts.

Similar issues arise when the whole matrix  $Q^*$  is approximated using Chebyshev semi-iteration. We illustrate the difficulty for lowest-order ( $\mathbb{P}_1$ ) elements on triangles. First note that  $Q^*$  is assembled from contributions on each element. If we again order the vertex degrees of freedom before the centroid degree of freedom then each element mass matrix is of the form

$$Q_T^* = \frac{\Delta_T}{12} \begin{bmatrix} 2 & 1 & 1 & 4 \\ 1 & 2 & 1 & 4 \\ 1 & 1 & 2 & 4 \\ 4 & 4 & 4 & 12 \end{bmatrix},$$

where  $\Delta_T$ ,  $T = 1, \dots, n_{el}$ , is the size of the  $T$ th triangular element. These element pressure mass matrices can be used to bound the eigenvalues of  $\text{diag}(Q^*)^{-1}Q^*$  via the method described by Wathen [18]. Doing so shows that the eigenvalues of  $\text{diag}(Q^*)^{-1}Q^*$  are contained in  $[0, 3]$ , and indeed these bounds are tight. The presence of a zero eigenvalue, and a number of additional very small eigenvalues, means that any approximation of  $Q^*$  based on its diagonal, including Chebyshev semi-iteration, is unlikely to give good results, and this is what we see in practice. More generally, we have been unable to find a spectrally equivalent approximation to  $Q^*$  that is efficient, and so in the following we use the original sparse matrix  $Q^*$  in our preconditioning strategies.

**2.4. Reliable computation of the discrete inf–sup constant.** A typical strategy to estimate the inf–sup constant for (1) is to find the largest  $\gamma$  that satisfies (3), i.e., to find the smallest nonzero eigenvalue of the generalised eigenvalue problem

$$BA^{-1}B^T \mathbf{v} = \lambda Q^* \mathbf{v}. \quad (10)$$

However, in our case, Propositions 1 and 2 show that  $\mathbf{k}$  lies in the nullspaces of both  $B^T$  and  $Q^*$ , which means that this generalised eigenvalue problem is singular, i.e., any  $\lambda \in \mathbb{R}$  satisfies (10) when  $\mathbf{v} = \mathbf{k}$ . It is known that generalised eigenvalue problems with singular pencils are challenging to solve numerically [8], and additional checks must be performed to ensure that an estimate of  $\gamma$  is not associated with the eigenvector  $\mathbf{k}$ . In practice we find that standard methods for computing eigenvalues of sparse matrices may struggle to accurately compute these eigenvalues, precisely because  $BA^{-1}B^T$  and  $Q^*$  are singular.

On the other hand, the EST-MINRES approach proposed in [14] is much more robust and gives consistently reliable results. The intuition is that by ensuring that any solves with  $Q^*$  are orthogonal to  $\mathbf{k}$  within the preconditioned MINRES method, so that the MINRES basis vectors are orthogonal to  $\mathbf{w}$ , as described in section 2.2, we instead solve (10) for  $\mathbf{v} \perp \mathbf{k}$ .

We illustrate the EST-MINRES inf-sup constant estimates using two representative test problems that we describe below. All numerical results were obtained using T-IFISS [2] (for triangular elements) and a IFISS3D [13] (for cubic elements). The stopping criterion for preconditioned MINRES is a reduction of the norm of the preconditioned residual by eight orders of magnitude, i.e.,  $\|\mathbf{r}_k\|_{\mathcal{P}^{-1}}/\|\mathbf{r}_0\|_{\mathcal{P}^{-1}} < 10^{-8}$ . We apply the preconditioner (4) with  $\mathbf{M} = \mathbf{A}$  and  $M_S = Q^*$ . Although this preconditioner can be expensive to apply, because it involves exact solves with  $\mathbf{A}$ , we have used it here to more clearly illustrate the key findings of this section, namely, that (4) with  $M_S = Q^*$  is an effective preconditioner for augmented Taylor–Hood problems, despite the singularity of  $Q^*$ , and that EST-MINRES provides reliable approximations to  $\gamma$ , the discrete inf-sup constant in (3). However, we note that it is possible to replace  $\mathbf{A}$  by, e.g., an algebraic multigrid method such as the HSL code MI20 [9]. With this AMG approximation, we were able to solve a 3D problem with nearly  $10^6$  degrees of freedom in under 10 seconds on a standard desktop machine.

**Test problem 1** (two-dimensional enclosed flow). Our first example is a classical driven-cavity flow in the square domain  $D = [-1, 1]^2$ . A Dirichlet no-flow condition is imposed on the bottom and side boundaries, while on the lid the nonzero tangential velocity is  $u_y = 1 - x^4$ . The domain is subdivided uniformly into  $n^2$  bisected squares. We use both the standard  $\mathbb{P}_2$ – $\mathbb{P}_1$  Taylor–Hood mixed approximation, and the augmented  $\mathbb{P}_2$ – $\mathbb{P}_1^*$  approximation. The two components of the pressure solution for the  $\mathbb{P}_2$ – $\mathbb{P}_1^*$  approximation, computed in the case  $n = 32$ , are illustrated in Fig. 1. The centroid pressure field is concentrated in the two corners where the pressure is singular, and the centroid pressures are an order of magnitude smaller than the vertex pressure in all elements. Consequently, the overall pressure field is visually identical to the  $\mathbb{P}_1$  pressure field shown in the left plot.

**Test problem 2** (three-dimensional enclosed flow). Our second problem is a three-dimensional version of driven-cavity flow. The domain is now  $D = [-1, 1]^3$ . As in the previous example, the flow is enclosed, but now the nonzero tangential velocity  $u_y = (1 - x^4)(1 - z^4)$  is specified on the top of the cavity. The domain is subdivided uniformly into  $n^3$  cubic elements, and we use  $\mathbb{Q}_2$ – $\mathbb{Q}_1$  and  $\mathbb{Q}_2$ – $\mathbb{Q}_1^*$  approximations.

Table 1 shows preconditioned MINRES iteration counts and EST-MINRES discrete inf-sup constant approximations for Example 1. We first note that for both the  $\mathbb{P}_2$ – $\mathbb{P}_1$  and  $\mathbb{P}_2$ – $\mathbb{P}_1^*$  approximations the iteration counts are quite similar and are mesh independent.



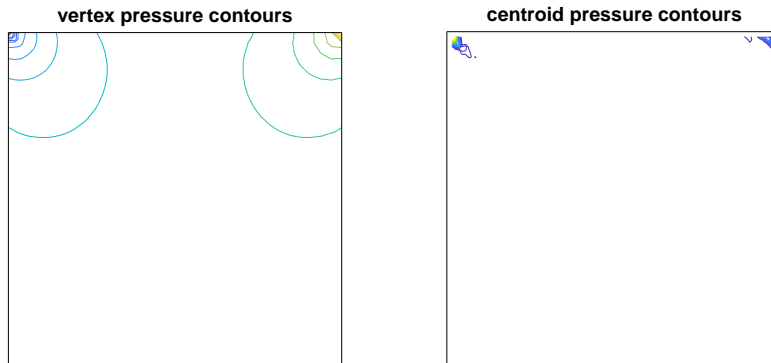


FIGURE 1. Representative  $\mathbb{P}_2\text{-}\mathbb{P}_1^*$  pressure field solution for the cavity flow in Example 1 computed on a uniform mesh with 2048 right-angled triangles and 1089 vertices.

Grid	$\mathbb{P}_2\text{-}\mathbb{P}_1$				$\mathbb{P}_2\text{-}\mathbb{P}_1^*$			
	Velocity dof	Pressure dof	Iters	$\gamma^2$	Velocity dof	Pressure dof	Iters	$\gamma^2$
4	2178	289	37	0.1947	2178	801	42	0.1397
5	8450	1089	37	0.1926	8450	3137	42	0.1396
6	33282	4225	39	0.1911	33282	12417	40	0.1395
7	132098	16641	37	0.1898	132098	49409	40	0.1395
8	526338	66049	37	0.1888	526338	197121	40	0.1395

TABLE 1. Preconditioned MINRES iterations and discrete inf-sup constant approximations for Example 1 and preconditioner (4) with  $\mathbf{M} = \mathbf{A}$  and  $M_S = Q^*$ .

In both cases the inf-sup constant approximations also appear to be converging from above. The approximation for  $\mathbb{P}_2\text{-}\mathbb{P}_1^*$  elements appears to rapidly converge to four digits, indicating that even a relatively coarse grid is sufficient to obtain an approximation to the discrete inf-sup constant. However, the approximation for  $\mathbb{P}_2\text{-}\mathbb{P}_1$  elements appears to converge more slowly. We also note that the two approaches give different inf-sup constant estimates, at least for the grids shown here. This is not so surprising as the matrices in (3) depend on the choice of finite element spaces.

Fig. 2 plots the inf-sup approximations at each iteration of preconditioned MINRES for Example 1. We see that a good approximation of the inf-sup constant is obtained after 20–25 iterations. It is again clear that for the enriched Taylor–Hood approximations we obtain very similar approximations for all grids.

The results for Example 2 are broadly similar, as can be seen from Table 2 and Fig. 3. The preconditioned MINRES iteration counts are mesh independent and, for all but the coarsest mesh, are almost identical for the two element pairs. The discrete inf-sup constant approximations again appear to converge from above. Now, at least for the grids presented here, the estimates of  $\gamma^2$  for Taylor–Hood elements seem to “track” the augmented Taylor–Hood estimates, i.e., the Taylor–Hood approximation on grid  $j$  is almost the same as the augmented Taylor–Hood estimate on grid  $j - 1$ . We also see from Fig. 2, which plots the inf-sup approximations at each iteration of preconditioned

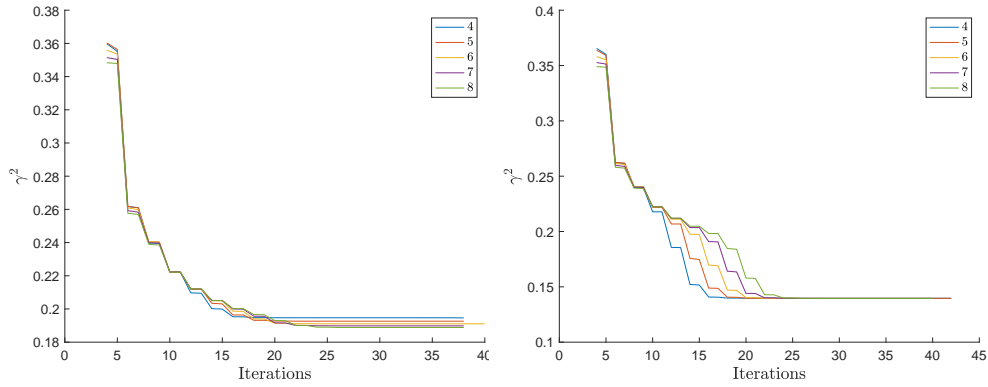


FIGURE 2. EST-MINRES estimates of the discrete inf-sup constant  $\gamma^2$  at each iteration for Example 1 with  $\mathbb{P}_2\text{-}\mathbb{P}_1$  (left) and  $\mathbb{P}_2\text{-}\mathbb{P}_1^*$  (right) elements for the grids specified in Table 1. The preconditioner is (4) with  $\mathbf{M} = \mathbf{A}$  and  $M_S = Q^*$ .

Grid	$\mathbb{Q}_2\text{-}\mathbb{Q}_1$				$\mathbb{Q}_2\text{-}\mathbb{Q}_1^*$			
	Velocity dof	Pressure dof	Iters	$\gamma^2$	Velocity dof	Pressure dof	Iters	$\gamma^2$
3	2187	125	45	0.1128	2187	189	48	0.1122
4	14739	729	51	0.1122	14739	1241	52	0.1115
5	107811	4913	51	0.1116	107811	9009	52	0.1110

TABLE 2. Preconditioned MINRES iterations and discrete inf-sup constant approximations for Example 2 and preconditioner (4) with  $\mathbf{M} = \mathbf{A}$  and  $M_S = Q^*$ .

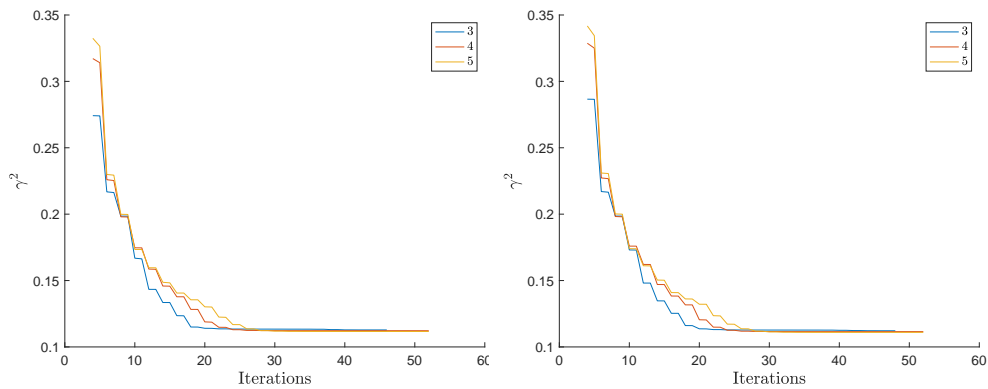


FIGURE 3. EST-MINRES estimates of the discrete inf-sup constant  $\gamma^2$  at each iteration for Example 2 with  $\mathbb{Q}_2\text{-}\mathbb{Q}_1$  (left) and  $\mathbb{Q}_2\text{-}\mathbb{Q}_1^*$  (right) elements for the grids specified in Table 2. The preconditioner is (4) with  $\mathbf{M} = \mathbf{A}$  and  $M_S = Q^*$ .

MINRES, that the discrete inf-sup constant is already reasonably well approximated after 25 iterations.

### 3. TWO-FIELD PRESSURE PRECONDITIONING STRATEGIES FOR OSEEN FLOW.

The focus of this section is the discrete matrix system

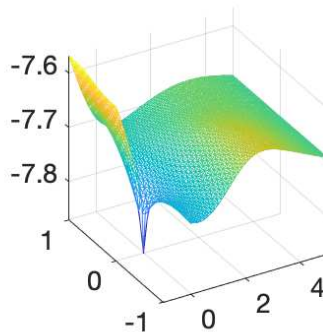
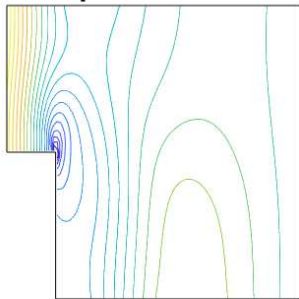
$$\begin{bmatrix} \mathbf{F} & B^T \\ B & 0 \end{bmatrix} \begin{bmatrix} \mathbf{u} \\ \mathbf{p} \end{bmatrix} = \begin{bmatrix} \mathbf{f} \\ \mathbf{g} \end{bmatrix}, \quad (11)$$

that arises from applying fixed point iteration, see for example [5, equation (8.46)], to the spatially discretised Navier–Stokes equations. The unknown coefficient vector involves the discrete velocity vector  $\mathbf{u} \in \mathbb{R}^{n_u}$  and the two-field pressure vector  $\mathbf{p} \in \mathbb{R}^{n_p}$ . The nonsymmetry of the matrix  $\mathbf{F}$  means that the iterative solver of choice is GMRES (see [5, section 9.1]) together with a block preconditioning operator of the form

$$\mathcal{M} = \begin{bmatrix} \mathbf{M} & B^T \\ 0 & -M_S \end{bmatrix}, \quad (12)$$

where  $\mathbf{M}$  is an optimal complexity (multigrid) operator effecting the action of the inverse of the matrix  $\mathbf{F}$  and  $M_S$  is an optimal complexity approximation of the Schur complement matrix  $B\mathbf{F}^{-1}B^T$ . We will discuss results for two representative flow problems herein.

**vertex pressure contours**



**centroid pressure contours**

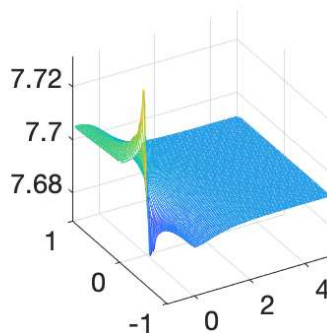
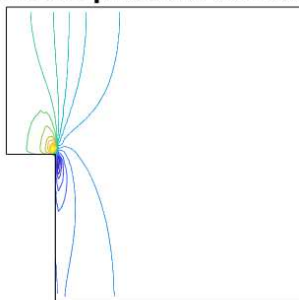


FIGURE 4. Representative  $\mathbb{P}_2\text{--}\mathbb{P}_1^*$  pressure field solution for flow over a step ( $\mathcal{R} = 100$ ) computed on a uniform mesh with 5632 right-angled triangles and 2945 vertices.

**Test problem 3** (flow over a step). We consider an inflow–outflow problem defined on the domain  $D = [-1, 0] \times [0, 1] \cup [0, 5] \times [-1, 1]$  with the viscosity parameter  $\nu$  set to

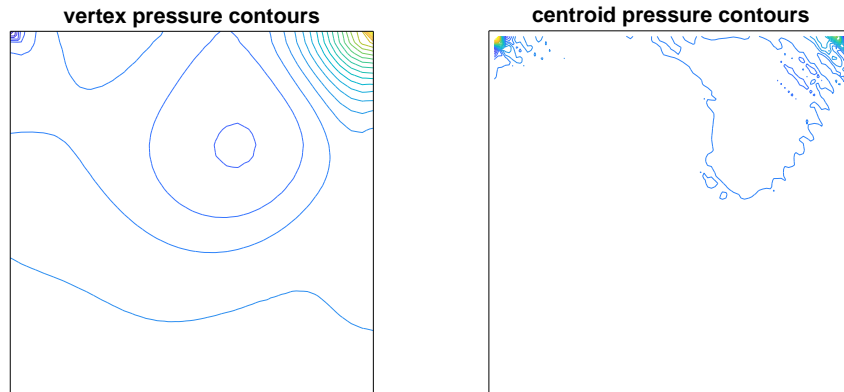


FIGURE 5. Representative  $\mathbb{P}_2\text{--}\mathbb{P}_1^*$  pressure field solution for cavity flow ( $\mathcal{R} = 200$ ) computed on a uniform mesh with 2048 right-angled triangles and 1089 vertices.

$1/50$  and a parabolic velocity  $u_x = 4y(1 - y)$  specified on the inflow boundary  $x = -1$ . The construction of the standard weak formulation (see [5, p. 127]) gives rise to a natural boundary condition that fixes the hydrostatic pressure level by weakly enforcing a zero mean pressure at the outflow boundary  $x = 5$ . (The other boundary conditions are associated with fixed walls.) We consider the discrete system (11) that results after 5 fixed-point iterations of the discretised Navier–Stokes system starting from the corresponding Stokes flow solution. We generate solutions using  $\mathbb{Q}_2\text{--}\mathbb{Q}_1$  or  $\mathbb{P}_2\text{--}\mathbb{P}_1$  augmented Taylor–Hood mixed approximation with the domain subdivided uniformly into (bisected) squares. The resulting system (11) is singular with the one-dimensional pressure nullspace described in section 2. The two components of the pressure solution computed on a representative  $\mathbb{P}_2\text{--}\mathbb{P}_1$  mesh are illustrated in Fig. 4. The centroid pressure values are an order of magnitude smaller than the vertex pressure in all the elements—they provide the “corrections” to the vertex pressures that are needed to ensure local (elementwise) conservation of mass.

**Test problem 4** (two-dimensional enclosed flow). We consider the classical driven-cavity enclosed flow problem defined on the domain  $D = [-1, 1]^2$  with the viscosity parameter  $\nu$  set to  $1/100$  and a nonzero tangential velocity  $u_y = 1 - x^4$  specified on the top of the cavity. We take  $\mathbb{P}_2\text{--}\mathbb{P}_1$  augmented Taylor–Hood mixed approximation with the domain subdivided uniformly into  $n^2$  bisected squares. We consider the discrete system (11) that arises after 5 fixed-point iterations starting from the corresponding Stokes flow solution. The discrete system is singular with a two-dimensional pressure nullspace, corresponding to a constant vertex pressure and a constant centroid pressure. The two components of the pressure solution computed in the case  $n = 32$  are illustrated in Fig. 5. Since the centroid pressure values are an order of magnitude smaller than the vertex pressure in all elements, the overall pressure field is visually identical to the  $\mathbb{P}_1$  pressure field shown in the left plot. As might be anticipated, the centroid “correction” pressure field is concentrated in the two corners where the pressure is singular.

**3.1. Pressure convection-diffusion preconditioning for Oseen flow.** There are two alternative ways of approximating the key matrix  $B\mathbf{F}^{-1}B^T$  in the case that  $B^T$  is generated by a two-field pressure approximation so that  $B^T = [B_1^T, B_0^T]$ . The focus will be on pressure convection-diffusion (PCD) preconditioning in this section. Both of the

Schur complement approximations can be motivated by starting with the Oseen matrix operator (11) and observing that the diagonal blocks of  $\mathbf{F}$  are discrete representations of the convection–diffusion operator

$$\mathcal{L} = -\nu\nabla^2 + \vec{w}_h \cdot \nabla, \quad (13)$$

defined on the velocity space. In practical calculations  $\nu > 0$  is proportional to the inverse of the flow Reynolds number and  $\vec{w}_h$  is the discrete approximation to the flow velocity computed at the most recent nonlinear iteration. The PCD approximation supposes that there is an analogous operator to (13), namely

$$\mathcal{L}_p = (-\nu\nabla^2 + \vec{w}_h \cdot \nabla)_p \quad (14)$$

defined on the two components of the augmented pressure space.

To this end, defining  $\{\phi_j\}_{j=1}^{n_1}$  to be the basis for the  $C^0$  pressure discretization, we construct matrices  $Q_1$  and  $F_1$  so that

$$\begin{aligned} Q_1 &= [q_{1,ij}], & q_{1,ij} &= \int_{\Omega} \phi_j \phi_i \\ F_1 &= [f_{1,ij}], & f_{1,ij} &= \nu \int_{\Omega} \nabla \phi_j \cdot \nabla \phi_i + \int_{\Omega} (\vec{w}_h \cdot \nabla \phi_j) \phi_i. \end{aligned}$$

We then note that if the commutator with the divergence operator

$$\mathcal{E} = \nabla \cdot (-\nu\nabla^2 + \vec{w}_h \cdot \nabla) - (-\nu\nabla^2 + \vec{w}_h \cdot \nabla)_p \nabla \cdot$$

is small then we have the approximation

$$0 \approx (Q_1^{-1} B_1) (\mathbf{M}^{-1} \mathbf{F}) - (Q_1^{-1} F_1) (Q_1^{-1} B_1) \quad (15)$$

where  $\mathbf{M}$  is the diagonal of the mass matrix associated with the basis representation of the velocity space.<sup>1</sup> Rearranging (15) gives the first Schur complement approximation

$$B_1 \mathbf{F}^{-1} B^T \approx Q_1 F_1^{-1} (B_1 \mathbf{M}^{-1} B^T). \quad (16)$$

A discrete version of  $\mathcal{L}_p$  for the piecewise constant pressure space can be generated by considering the jumps in pressure across inter-element boundaries; see [5, pp.268–370]. To this end, defining  $\{\varphi_j\}_{j=1}^{n_0}$  to be the (indicator function) basis for the discontinuous pressure, we construct matrices  $Q_0$  and  $F_0$  via

$$\begin{aligned} Q_0 &= [q_{0,ij}], & q_{0,ij} &= \int_{\Omega} \varphi_j \varphi_i = \begin{cases} |T_i| & \text{if } i = j, \\ 0 & \text{otherwise,} \end{cases} \\ F_0 &= [f_{0,ij}], & f_{0,ij} &= \nu \sum_{T \in \mathcal{T}_h} \int_T \nabla \varphi_j \cdot \nabla \varphi_i + \sum_{T \in \mathcal{T}_h} \int_T (\vec{w}_h \cdot \nabla \varphi_j) \varphi_i \end{aligned}$$

and note that if the commutator with the divergence operator is small then we have

$$0 \approx (Q_0^{-1} B_0) (\mathbf{M}^{-1} \mathbf{F}) - (Q_0^{-1} F_0) (Q_0^{-1} B_0), \quad (17)$$

suggesting the second Schur complement approximation

$$B_0 \mathbf{F}^{-1} B^T \approx Q_0 F_0^{-1} (B_0 \mathbf{M}^{-1} B^T). \quad (18)$$

---

<sup>1</sup>The inverse of  $\mathbf{M}$  is a dense matrix. The diagonal of  $\mathbf{M}$  is a spectrally equivalent matrix operator with a sparse (diagonal) inverse.

Combining (16) with (18) then gives a two-field PCD approximation

$$B\mathbf{F}^{-1}B^T \approx M_S := \begin{bmatrix} Q_1 & 0 \\ 0 & Q_0 \end{bmatrix} \begin{bmatrix} F_1^{-1} & 0 \\ 0 & F_0^{-1} \end{bmatrix} B\mathbf{M}^{-1}B^T. \quad (19)$$

Two features of the PCD approximation (19) are worth noting. The first point is that the coupling between the pressure components is represented by the  $2 \times 2$  block matrix  $B\mathbf{M}^{-1}B^T$  rather than by the pressure mass matrix  $Q^*$  (the coupling term  $R$  is absent). The second key point is that the matrices  $M_S$  and  $B\mathbf{F}^{-1}B^T$  have the same nullspace, independent of the nature of underlying flow problem that is being solved.

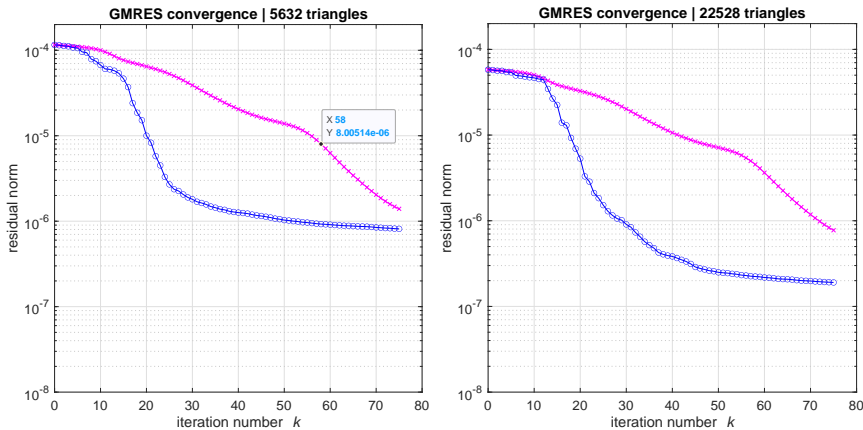


FIGURE 6. Absolute residual reduction for test problem 3 when computing  $\mathbb{P}_2\text{--}\mathbb{P}_1^*$  solutions using preconditioners  $\mathcal{M}_1$  (x) or  $\mathcal{M}_2$  (o) on two nested meshes.

The PCD approximation in (19) is imperfect in practice. To illustrate this, representative convergence histories that arise in solving the inflow-outflow problem using  $\mathbb{P}_2\text{--}\mathbb{P}_1^*$  approximation (shown in Fig. 4) are presented in Fig. 6. Taking the solution from the previous Picard iteration as the initial guess, we note that the initial residual norm of the target matrix system (11) is close to  $10^{-4}$  independent of the spatial discretisation. Convergence plots are presented for two preconditioning strategies, namely

$$\mathcal{M}_1 = \begin{bmatrix} \mathbf{F} & B^T \\ 0 & -\frac{1}{\nu}Q^* \end{bmatrix}, \quad \mathcal{M}_2 = \begin{bmatrix} \mathbf{F} & B^T \\ 0 & -M_S \end{bmatrix}, \quad (20)$$

with  $M_S$  defined in (19). The first strategy is the block triangular extension of the Stokes preconditioning strategy discussed in section 2. We note that the resulting convergence is very slow—around 50 iterations are required to reduce the residual norm by an order of magnitude—but is independent of the discretisation level. In contrast we see that the PCD preconditioning strategy has two distinctive phases of convergence behaviour. An initial phase of relatively fast convergence is followed by a secondary phase where GMRES stagnates. We hypothesise that this stagnation is a consequence of the ill-conditioning of the eigenvectors of the matrix operator  $M_S$ . A notable feature is that the onset of the stagnation is delayed when solving the same problem on a finer grid. The two-phase convergence behaviour is ubiquitous—the same pattern is seen using rectangular elements and the stagnation does not go away when the viscosity parameter is increased from  $1/50$  to  $1/5$ . An alternative strategy is clearly needed!

One way of designing a more robust PCD preconditioning strategy for a two-field pressure approximation is to exploit the fast convergence of the PCD approximation for the unaugmented Taylor-Hood approximation. The starting point for such a strategy is to rewrite the system (11) in the form

$$\begin{bmatrix} \mathbf{F} & B_1^T & B_0^T \\ B_1 & 0 & 0 \\ B_0 & 0 & 0 \end{bmatrix} \begin{bmatrix} \mathbf{u} \\ \mathbf{p}_1 \\ \mathbf{p}_0 \end{bmatrix} = \begin{bmatrix} \mathbf{f} \\ \mathbf{0} \\ \mathbf{0} \end{bmatrix}. \quad (21)$$

The proposed solution algorithm is then a two-stage process.

- **Input:** residual reduction tolerance  $\eta$

Step I Generate a PCD solution to the *reduced system*

$$\begin{bmatrix} \mathbf{F} & B_1^T \\ B_1 & 0 \end{bmatrix} \begin{bmatrix} \mathbf{u}_1 \\ \mathbf{q}_1 \end{bmatrix} = \begin{bmatrix} \mathbf{f} \\ \mathbf{0} \end{bmatrix} \quad (22)$$

using the Schur complement approximation (15), stopping the GMRES iteration when the residual is reduced by a factor of  $10\eta$ .

Step II Generate a solution to the target system (21) with residual tolerance  $\eta$  using preconditioning strategy  $\mathcal{M}_1$  in (20) with the refined initial guess  $[\mathbf{u}_1^*, \mathbf{q}_1^*, \mathbf{0}]$ .

- **Output:** refined solution  $[\mathbf{u}^*, \mathbf{p}_1^*, \mathbf{p}_0^*]$

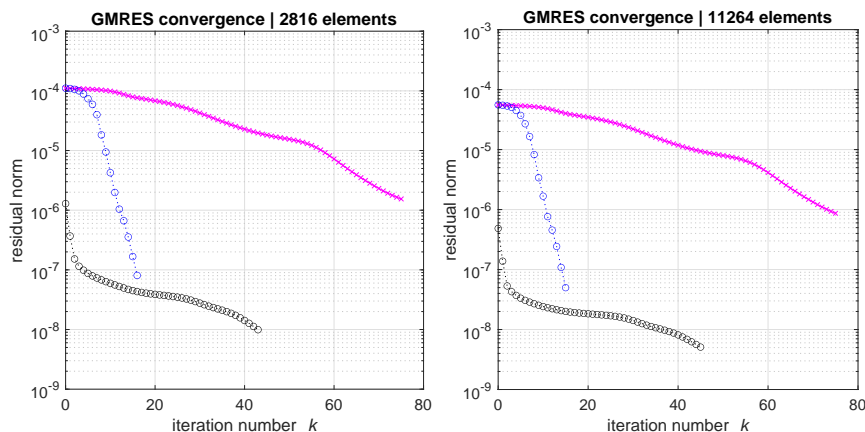


FIGURE 7. Absolute residual reduction for test problem 1 when computing  $\mathbb{Q}_2\text{--}\mathbb{Q}_1^*$  solutions using using preconditioners  $\mathcal{M}_1$  (x) or refined PCD (o) on two nested meshes.

Sample results generated using this strategy with tolerance  $\eta$  set to  $10^{-4}$  are presented in Fig. 7. Sample results for the second test problem are presented in Fig. 8. The results in Fig. 7 and Fig. 8 are representative of the two-stage convergence profiles that are generated when solving these test problems at other Reynolds numbers. Our experience is that the level of residual reduction is perfectly robust with regards to the spatial discretisation—typically giving smaller iteration counts when the mesh resolution is increased (a known feature of PCD preconditioning). The convergence rates of both stages of the algorithm deteriorate slowly when the Reynolds number is increased. Our strategy for terminating the first stage of the iteration is motivated by the following result.

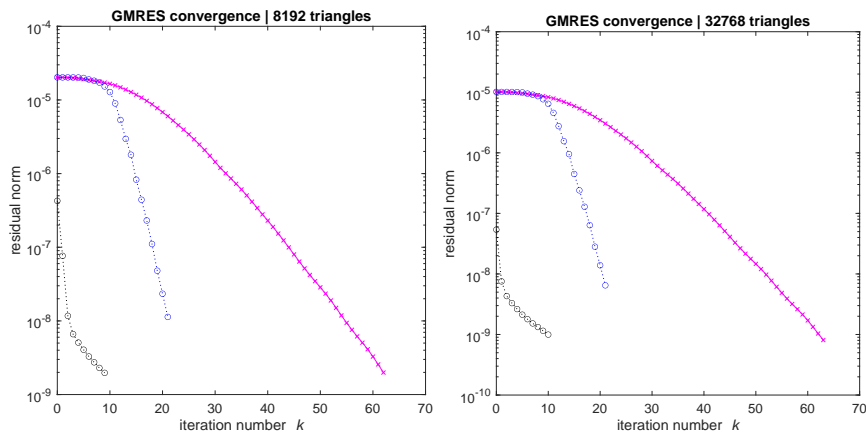


FIGURE 8. Absolute residual reduction for test problem 2 when computing  $\mathbb{P}_2\text{-}\mathbb{P}_1^*$  solutions using preconditioners  $\mathcal{M}_1(\mathbf{x})$  (x) or refined PCD (o) on two nested meshes.

**Proposition 4.** *The residual error  $\|\mathbf{z}^*\|$  associated with the intermediate solution  $[\mathbf{u}_1^*, \mathbf{q}_1^*, \mathbf{0}]$  to the discrete system (21) satisfies the bound*

$$\|\mathbf{z}^*\|^2 \leq 100\eta^2 \|\mathbf{f}\|^2 + \|B_0 \mathbf{u}_1^*\|^2, \quad (23)$$

where  $\|\mathbf{f}\|$  is the initial residual error associated with a zero initial vector.

*Proof.* The vector  $\mathbf{z}^*$  associated with the intermediate solution is the three-component vector

$$\begin{bmatrix} \mathbf{r}^* \\ \mathbf{r}_1^* \\ \mathbf{r}_0^* \end{bmatrix} = \begin{bmatrix} \mathbf{f} \\ \mathbf{0} \\ \mathbf{0} \end{bmatrix} - \begin{bmatrix} \mathbf{F} & B_1^T & B_0^T \\ B_1 & 0 & 0 \\ B_0 & 0 & 0 \end{bmatrix} \begin{bmatrix} \mathbf{u}_1^* \\ \mathbf{q}_1^* \\ \mathbf{0} \end{bmatrix}. \quad (24)$$

The stopping test for solving the reduced system ensures that

$$\|\mathbf{r}^*\|^2 + \|\mathbf{r}_1^*\|^2 \leq 100\eta^2 \|\mathbf{f}\|^2. \quad (25)$$

Thus we have

$$\|\mathbf{z}^*\|^2 = \|\mathbf{r}^*\|^2 + \|\mathbf{r}_1^*\|^2 + \|\mathbf{r}_0^*\|^2 \leq 100\eta^2 \|\mathbf{f}\|^2 + \|B_0 \mathbf{u}_1^*\|^2. \quad (26)$$

□

The bound (23) has two terms on the right-hand side. While the first term can be controlled by reducing  $\eta$ , the second term measures the local incompressibility of the intermediate Taylor–Hood solution  $\|B_0 \mathbf{u}_1^*\|^2 = \sum_j (\int_{T_j} \nabla \cdot \vec{u}_h^*)^2$ , where  $\vec{u}_h^*$  is the expansion of the coefficient vector  $\mathbf{u}_1^*$  in the basis of the velocity approximation space. Setting  $\eta = 10^{-4}$  we see that the second term saturates the residual error and the residual error jumps up when the switch is made from the first to the second step of the algorithm. This “transition” jump in the residual norm is clearly evident in the convergence plots. The convergence in the second step is rapid initially but eventually mirrors the rate observed for  $\mathcal{M}_1$  approximation with a standard starting guess.



**3.2. Least square commutator approximation for Oseen flow.** A second way of approximating the key matrix  $B\mathbf{F}^{-1}B^T$  in the case that  $B^T$  is generated by a two-field pressure approximation is given by the least-squares commutator (LSC) preconditioner

$$B\mathbf{F}^{-1}B^T \approx M_S = (B\mathbf{H}^{-1}B^T)(BM^{-1}\mathbf{F}\mathbf{H}^{-1}B^T)^{-1}(BM^{-1}B^T). \quad (27)$$

The attractive feature of LSC is that the construction of  $M_S$  is completely algebraic. The only technical issue is the need to make adjustments on rows and columns associated with tangential velocity degree of freedom adjacent to inflow and fixed wall boundaries. These adjustments are associated with a diagonal scaling matrix  $\mathbf{D}$  so that  $\mathbf{H} = \mathbf{D}^{-1/2}\mathbf{M}\mathbf{D}^{-1/2}$ . Full details can be found in [5, pp. 376–379]).

The LSC approximation (27) is also far from perfect when using triangular elements.<sup>2</sup> To illustrate this, representative convergence histories that arise in solving the inflow-outflow problem using  $\mathbb{P}_2\text{--}\mathbb{P}_1^*$  approximation are presented in Fig. 9. Convergence plots are presented for two preconditioning strategies, namely the refined PCD from the previous section and

$$\mathcal{M}_3 = \begin{bmatrix} \mathbf{F} & B^T \\ 0 & -M_S \end{bmatrix}, \quad (28)$$

with  $M_S$  defined in (27).

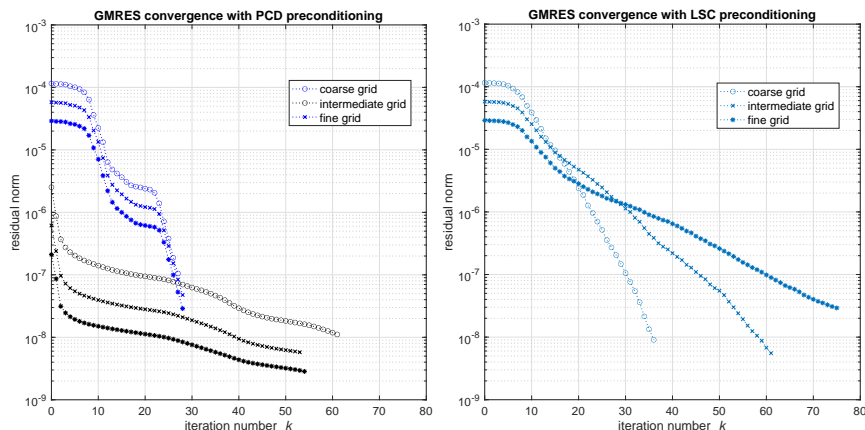


FIGURE 9. Absolute residual reduction for test problem 1 when computing  $\mathbb{P}_2\text{--}\mathbb{P}_1^*$  solutions using refined PCD (left) or preconditioner  $\mathcal{M}_3$  (right) on three nested meshes.

The PCD convergence histories are comparable with those generated using square elements (cf. Fig. 7). The associated cpu times for the solution on the intermediate grid with  $2 \times 11264$  elements were 13 seconds for the first step (28 iterations) and 26 seconds for the second step (53 iterations). The LSC preconditioning strategy is not robust—the convergence rate deteriorates with increasing grid refinement. The cpu time for generating the LSC solution on the intermediate grid was over 100 seconds (61 iterations).

<sup>2</sup>The strategy is designed for tensor-product approximation spaces. It gives good results in the case of  $\mathbb{Q}_2\text{--}\mathbb{Q}_1^*$ .

#### 4. CONCLUSIONS

Two-level pressure approximation for incompressible flow problems offer the prospect of accurate approximation with minimal computational overhead. Derived quantities of practical importance such as the mean wall shear stress are likely to be computed much more precisely if incompressibility is enforced locally.<sup>3</sup> However, the augmented pressure space causes some challenges for the linear algebra, because constant functions can be expressed using either the usual (continuous) Taylor–Hood pressure space, or the augmented piecewise constant pressure space. Specifically, the pressure mass matrix becomes singular, and care should be taken to carefully construct and apply preconditioners that involve this matrix. Care should also be exercised when approximating the discrete inf-sup constant, and we find that naive approaches are not always reliable. On the other hand, the approximation implemented in EST-MINRES is robust. Our computational experimentation indicates that our two-stage PCD strategy could be the best way of iteratively solving two-level pressure discrete linear algebra systems in the sense of algorithmic reliability and computational efficiency.

#### REFERENCES

- [1] M. BENZI, G. H. GOLUB, AND J. LIESEN, *Numerical solution of saddle point problems*, Acta Numer., 14 (2005), pp. 1–137.
- [2] A. BESPALOV, L. ROCCHI, AND D. SILVESTER, *T-IFISS: a toolbox for adaptive FEM computation*, Comput. Math. Appl., 81 (2021), pp. 373–390.
- [3] D. BOFFI, F. BREZZI, AND M. FORTIN, *Mixed Finite Element Methods and Applications*, Springer Series in Computational Mathematics 44, Springer, Berlin, 2013.
- [4] D. BOFFI, N. CAVALLINI, F. GARDINI, AND L. GASTALDI, *Local mass conservation of Stokes finite elements*, J. Sci. Comput., 52 (2012), pp. 383–400.
- [5] H. ELMAN, D. SILVESTER, AND A. WATHEN, *Finite Elements and Fast Iterative Solvers: with Applications in Incompressible Fluid Dynamics*, Oxford University Press, Oxford, UK, 2014. Second Edition.
- [6] P. GRESHO, R. LEE, S. CHAN, AND J. LEONE, *A new finite element for incompressible or Boussinesq fluids*. In *Third International Conference on Finite Elements in Flow Problems*, pages 204–215. Wiley, New York, 1981.
- [7] D. GRIFFITHS, *The effect of pressure approximation on finite element calculations of incompressible flows*. In K.W. Morton and M.J. Baines, editors, *Numerical Methods for Fluid Dynamics*, pages 359–374. Academic Press, San Diego, 1982.
- [8] M. E. HOCHSTENBACH, C. MEHL, AND B. PLESTENJAK, *Solving singular generalized eigenvalue problems by a rank-completing perturbation*, SIAM J. Matrix Anal. Appl., 40 (2019), pp. 1022–1046.
- [9] HSL, *A collection of Fortran codes for large scale scientific computation*. <http://www.hsl.rl.ac.uk/>.
- [10] Y. A. KUZNETSOV, *Efficient iterative solvers for elliptic finite element problems on nonmatching grids*, Russ. J. Numer. Anal. Math. Modelling, 10 (1995), pp. 187–211.
- [11] M. F. MURPHY, G. H. GOLUB, AND A. J. WATHEN, *A note on preconditioning for indefinite linear systems*, SIAM J. Sci. Comput., 21 (2000), pp. 1969–1972.
- [12] C. PAIGE AND M. SAUNDERS, *Solution of sparse indefinite systems of linear equations*, SIAM J. Numer. Anal., 12 (1975), pp. 617–629.
- [13] G. PAPANIKOS, C. E. POWELL, AND D. J. SILVESTER, *IFISS3D: A computational laboratory for investigating finite element approximation in three dimensions*. [arXiv:2209.13290 \[math.NA\]](https://arxiv.org/abs/2209.13290), 2022.

---

<sup>3</sup>See <https://personalpages.manchester.ac.uk/staff/david.silvester/lecture1.18.mp4> for a comparison of alternative strategies for computing the average shear stress for flow over a step at Reynolds number 200.

- [14] D. J. SILVESTER AND V. SIMONCINI, *An optimal iterative solver for symmetric indefinite systems stemming from mixed approximation*, ACM Trans. Math. Softw., 37 (2011). Article No. 42.
- [15] R. THATCHER, *Locally mass-conserving Taylor–Hood elements for two- and three-dimensional flow*, Int. J. Numer. Methods Fluids, 11 (1990), pp. 341–353.
- [16] R. THATCHER AND D. SILVESTER, *A locally mass conserving quadratic velocity, linear pressure element*. Manchester Centre for Computational Mathematics report 147, [arXiv:2001.11878 \[math.NA\]](https://arxiv.org/abs/2001.11878), 1987.
- [17] A. WATHEN AND T. REES, *Chebyshev semi-iteration in preconditioning for problems including the mass matrix*, Electron. Trans. Numer. Anal., 34 (2009), pp. 125–135.
- [18] A. J. WATHEN, *Realistic eigenvalue bounds for the Galerkin mass matrix*, IMA J. Numer. Anal., 7 (1987), pp. 449–457.

DEPARTMENT OF MATHEMATICS AND STATISTICS, UNIVERSITY OF STRATHCLYDE, GLASGOW, G1 1XH, UK

*Email address:* `jennifer.pestana@strath.ac.uk`

DEPARTMENT OF MATHEMATICS, UNIVERSITY OF MANCHESTER, OXFORD ROAD, MANCHESTER M13 9PL, UK

*Email address:* `d.silvester@manchester.ac.uk`